Insights into the Combination of Multilayered Hematite Nanowires with Thin-Film Silicon Photovoltaics in an All-Earth-Abundant Hybrid Tandem Device for Solar Water Splitting

Félix Urbain[1], Pengyi Tang[1,2], Vladimir Smirnov[3], Katharina Welter[3], Teresa Andreu[1,4], Friedhelm Finger[3], Jordi Arbiol[2,5], and Joan Ramón Morante[1,6]*

[1] IREC, Catalonia Institute for Energy Research, Jardins de les Dones de Negre 1, 08930 Sant Adrià de Besòs, Barcelona, Catalonia, Spain

[2] Catalan Institute of Nanoscience and Nanotechnology (ICN2), CSIC and BIST, Campus UAB, Bellaterra, 08193 Barcelona, Catalonia, Spain

[3] IEK-5 Photovoltaik, Forschungszentrum Jülich, D-52425, Jülich, Germany

[4] Universitat Politècnica de Catalunya, Jordi Girona 1–3, 08034 Barcelona, Catalonia, Spain

[5] ICREA, Pg. Lluís Companys 23, 08010 Barcelona, Catalonia, Spain

[6] Universitat de Barcelona, Martí i Franquès, 1, 08028 Barcelona, Catalonia, Spain

[*]**Corresponding author**: E-mail: furbain@irec.cat

Abstract

The concept of hybrid tandem device structures, which combine metal-oxides with thin-film semiconducting photoabsorbers holds great promises regarding large-scale, robust, and cost-effective bias-free photoelectrochemical water splitting (PEC-WS). This work highlights the important steps towards efficient coupling of high-performance hematite photoanodes with multijunction thin-film silicon photocathodes regarding high bias-free photocurrent density. The hybrid PEC-WS device was optimized by testing three types of multijunction silicon photocathodes with the hematite photoanode: a-Si:H/a-Si:H tandem, a-Si:H/a-Si:H/µc-Si:H and a-Si:H/µc-Si:H/µc-Si:H triple junction. We provide evidence that the multijunction structures offer a high flexibility for hybrid tandem devices, regarding tunable photovoltages and spectral matching. Furthermore, both photoanode and photocathode were tested under various electrolyte and light concentration conditions, respectively, with respect to their photoelectrochemical performance and stability. A 27 % enhancement in the solar-to-hydrogen conversion efficiency was observed by concentrating light from 100 to 300 mW/cm^2. Ultimately, we demonstrate bias-free water splitting with a photocurrent density of 4.6 mA/cm^2 (under concentrated illumination) paired with excellent operation stability for more than 24 hours of the all-earth-abundant and low-cost hematite/silicon tandem PEC-WS device.

1. Introduction

Photoelectrochemical water splitting (PEC-WS) recently has been standing at the pillory of critical studies judging the technology against PV-electrolyzer systems with respect to costs, efficiency, and stability.[1-3] It still remains to be proven what PEC-WS devices promised to offer compared to other production routes for solar hydrogen: (i) reduced costs through a higher level of integration, (ii) potentially higher solar-to-hydrogen efficiencies because of direct one-step conversion, and (iii) stable operation by employing chemically robust materials.[4] Regarding these requirements, hematite photoelectrodes appear as ideal candidates for PEC-WS devices, owing to their high natural abundance, low-cost and scalable deposition, adequate bandgap energy for WS (~ 2 eV), and photo-chemical robustness.[5] However, despite of many years of extensive research, hematite photoelectrodes could not live up to their promises, mainly due to low photovoltages, poor catalytic activity, and limited electrical conductivity. The present contribution aims to bring hematite back on track as PEC-WS material by making use of its beneficial properties while combining it with another earth-abundant and low-cost scalable photovoltaic material, namely thin-film silicon. In this monolithic tandem configuration, we seek to provide enough photovoltage to drive the water splitting reaction bias-free, while ensuring a high photocurrent through a good spectral matching of both light absorbers and improved catalytic properties for both the oxygen (OER) and hydrogen evolution reaction (HER). In particular, we combined an advanced hematite photoanode with multijunction thin-film silicon photocathodes. For the latter we optimized the absorber layer sequence in order to reach the best photocurrent-photovoltage tradeoff when coupled with the hematite absorber. The photoanode was composed of an ITO underlayer with Fe_2O_3 nanowires coated by a Fe_2TiO_5 (pseudobrookite) atomic layer and decorated with FeNiOOH nanodots, as recently reported by Tang *et al*.[6] By this integrated "one-chip" tandem approach, we circumvent the need for a counter electrode, which is physically separated from the photoelectrode and usually constituted of expensive materials.[7] As a consequence, the herein presented approach allows replacing costly and scarce OER materials, such as RuO_2, by cost-effective and earth-abundant hematite nanostructures. Another advantage of the herein proposed dual-absorber architecture is that the water splitting reactions occur directly at the conjoint semiconductor–liquid interfaces, which minimizes the number of junctions used, making the overall device simpler and potentially cheaper. Moreover, in contrast to previous approaches for unassisted PEC-WS using oxide-based hybrid tandem structures,[8-10] this study only investigated earth-abundant catalyst materials and analyzed the tandem system by robust stability testing. Furthermore, we introduced light concentration as an effective method to enhance the photoelectrochemical performance of both hybrid tandem partners, and thus to increase the achievable photocurrent density of the complete PEC-WS device.

2. Experimental

The fabrication of the ITO/Fe_2O_3/Fe_2TiO_5/FeNiOOH photoanode and the thin-film silicon multijunction photocathodes, respectively, as well as the optical, structural and compositional characterization of both hybrid tandem partners are described in detail in the Supplementary Information (SI) in Section 1.

For the (photo)-electrochemical characterization, both photoelectrodes were analyzed by means of linear sweep measurements (VMP3 Bio-Logic multi-channel potentiostat)

conducted at a scan rate of 10 mV/s in a three-electrode set-up using a Ag/AgCl (3 M KCl) reference electrode in aqueous NaOH electrolyte under ambient conditions. A 150 W AM 1.5G solar simulator (Solar Light Co., 16S-300-002 v4.0) was used as the light source, and the light density was calibrated using a thermopile (Gentec-EO, XLPF12-3S-H2-DO) coupled with an optical power meter (Gentec-EO UNO). The intensity of the light source was adjusted to match concentrated illumination conditions of 200 and 300 mW/cm^2 intensity, respectively, by varying the distance between the PEC-WS device and the solar simulator. For the hybrid tandem configuration both photoelectrodes were attached together, such that the glass sides of both respective substrates were in direct contact for good optical coupling. In the two-electrode configuration (chronoamperometry at 0 V applied bias) the complete PEC-WS device was sealed by thermoplastic resin paste surrounding the device except the two 1 cm^2 apertures defining the active areas for the solar-driven OER and HER, respectively. We applied nickel-based HER catalysts in this study. Both photoelectrodes were electrically contacted on the respective FTO coated glass substrate. Figure 1 schematically depicts the hybrid tandem device set-up under operation.

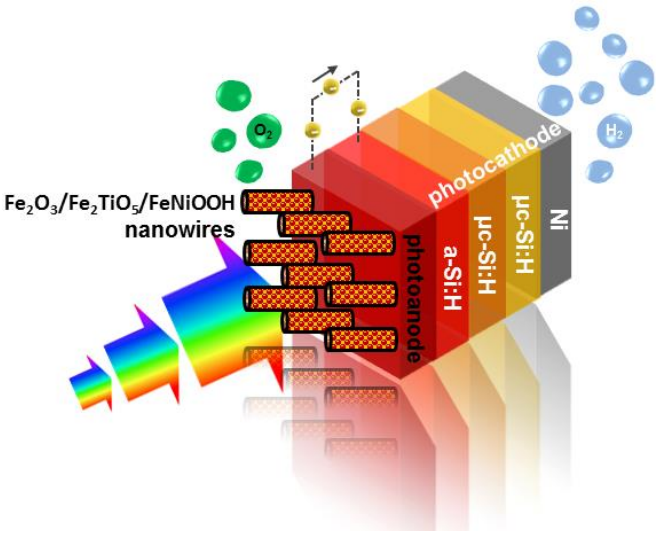

Figure 1. Schematic drawing of the hybrid tandem device under operation. The OER is performed by the ITO/Fe_2O_3/Fe_2TiO_5/FeNiOOH multilayered nanowire photoanode and the HER is powered by a multijunction thin-film silicon photocathode and a Ni-based catalyst. The light enters through the photoanode, as depicted.

3. Results

3.1.Multilayered hematite nanowire photoanode

The TEM and high-resolution (HRTEM) images of the hematite multi-layer nanowires are shown in Figure 2a and 2b, respectively. The coating of the Fe_2O_3 nanowire core by pseudobrookite shell can be seen from Figure 2d-f, which were deduced from the HRTEM image in Figure 2b and the corresponding fast-fourier-transform (FFT) spectrum in Figure 2c. As demonstrated in Ref. 6, this atomic layer can effectively suppress the charge recombination at the semiconductor junction interface, while the ITO underlayer enhances the electrical conductivity of the photoanodes resulting in a higher photocurrent density and an enhanced fill factor. The OER performance can be fostered by FeNiOOH nanodots (Figure 2b and Figure S1), which were deposited on the nanowire surface by photo-electrodeposition. By this, the number of active sites on the

nanowire surface can be increased, which is conducive to accelerated OER kinetics at the semiconductor-electrolyte interface, resulting in photocurrent densities of up to 2.2 mA/cm^2 at 1.23 V vs. RHE.[6] The electron energy loss spectroscopy (EELS) measurement of the as-developed nanowire structures on FTO glass/ITO substrate can be found in the SI in Figure S2.

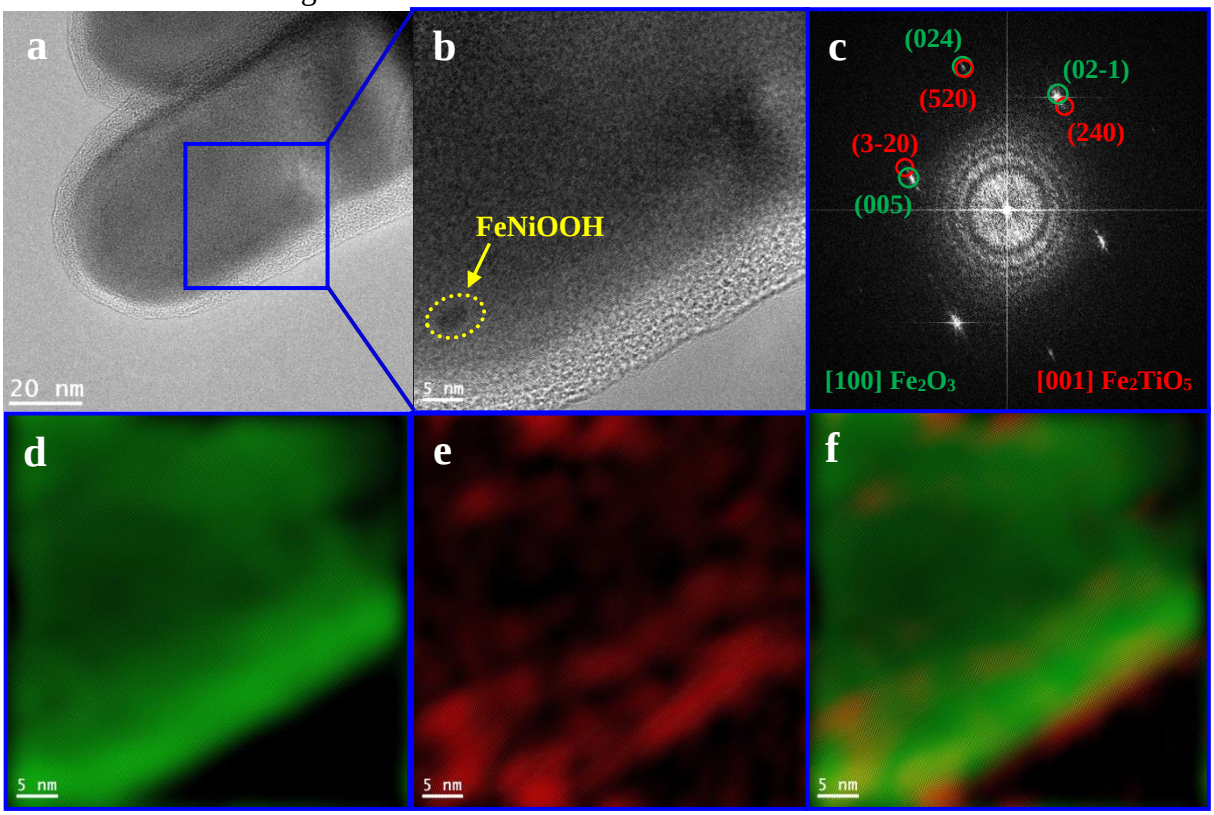

Figure 2. a) Low magnification TEM image of a multilayer nanowire. b) High resolution TEM of the blue squared area showing the hierarchal structure of the nanowire composite and the decoration of FeNiOOH nanodots, which are shown in more detail in Figure S1 in the SI. c) Corresponding fast-fourier-transform (FFT) spectrum of b) indicating that the nanowire is composed of hematite and pseudobrookite, being visualized along [100] and [001] directions, respectively. d) Phase map (green) of Fe_2O_3. e) Phase map (red) of Fe_2TiO_5. f) Mixed phase map of d) and e). All phase maps were obtained from b) after mask filtering the corresponding spots for each of the crystal phases in c) and obtaining their corresponding inverse fast-fourier-transform (IFFT) image. The IFFT RGB composite image in f) reveals the coating of pseudobrookite on the surface of the hematite nanowire.

3.2.Optical coupling of both tandem absorber partners

In the case of a dual-absorber tandem device, also the photocathode should fulfil particular requirements to enable unassisted overall water splitting: (i) provide enough additional photovoltage; (ii) be compatible with catalysts for efficient and stable HER; (iii) possess adequate band gap energy for efficient spectral matching with the hematite light absorber used for the OER. All these tasks can be performed by multijunction thin-film silicon photovoltaics made of hydrogenated amorphous (a-Si:H) and microcrystalline (µc-Si:H) silicon films. As already shown elsewhere,[7,11,12] "stacking" of a-Si:H and µc-Si:H absorber layers in monolithic multijunction solar cells (in contrast to crystalline silicon solar cells) allow for a highly precise adjustment of the

photovoltaic parameters, such as the photovoltage, without complex electrical connections, which would limit the practical application of PEC-WS systems, regarding compactness and customizability. Additionally, the thin-film silicon technology benefits from earth-abundance, low material consumption (absorber layer thickness below 3µm), light-weight, low-cost production, facile large-scale deposition, and can be combined with a wide range of HER catalysts.

We investigated three types of multijunction thin-film silicon cells for the combination with the hematite photoanode: a-Si:H/a-Si:H and a-Si:H/a-Si:H/µc-Si:H, and a-Si:H/µc-Si:H/µc-Si:H. The layer thicknesses for the individual a-Si:H and µc-Si:H sub-cells of the selected solar cells were optimized regarding high photovoltage and good current matching. In fact, it was shown that the photovoltage can be systematically tuned between 1.8 and 2.3 V with photovoltaic conversion efficiencies of up to 13.6 %. Therefore, the thin-film silicon multijunction solar cells offer a high flexibility for the usage as photocathodes in hybrid dual-absorber devices. Details on the preparation and application as photocathodes of the tested multijunction cells can be found in the Refs. 7 and 11, respectively and in the SI (Section 1). In the herein proposed hybrid tandem configuration for PEC-WS, the photoanode was placed before the photocathode, because the optical band gap energy of hematite is higher than that of thin-film silicon.[13] Quantum efficiencies (*QE*) of the tested thin-film silicon solar cells, with and without hematite photoanode as filter are shown in Figure 3 (left y-axis). These measurements allow gaining insights in the optical absorption and the carrier extraction efficiency of the photocathode in the hybrid tandem configuration, i.e. when the light first passes through the hematite absorber and then enters the thin-film silicon material. In the SI, the *QE* measurement and calculation is described in detail (Section 2).

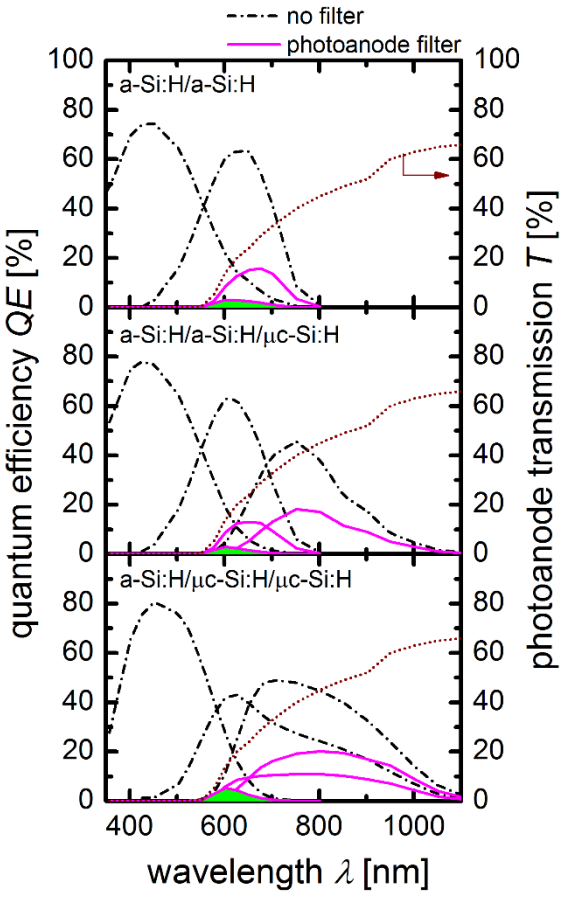

Figure 3. Left y-axis: Quantum efficiency (*QE*) for the three investigated thin-film silicon multijunction photocathodes: a-Si:H/a-Si:H, a-Si:H/a-Si:H/µc-Si:H, and a-Si:H/µc-Si:H/µc-Si:H. The dotted black lines show the measurements without filter and the purple lines show the calculated quantum efficiencies with the hematite placed before the silicon photocathodes. The calculations were based on the transmission measurement of the hematite photoanode, plotted on the right y-axis. For the convenience of the reader, the limiting sub-cell quantum efficiencies are indicated by green filling, which are shown in a magnified view in Figure S4.

The *QE* of the multijunction thin-film silicon sub cells with the hematite photoanode filter (purple curves) were calculated based on the measured *QE* (dashed black curves) and the measured transmission characteristic of the hematite photoanode filter, shown in Figure 3 (right y-axis). Please note that calculated and measured *QE* of the filtered multijunction solar cells were in very good agreement for the a-Si:H/a-Si:H solar cell, as shown in Figure S3 in the SI, which is why we used the calculated *QE* for all investigated cell types. As apparent from Figure 3 (left y-axis), the hematite material significantly reduced the *QE* of the three tested thin-film silicon structures in the complete investigated wavelength range, i.e. from 350–1100 nm. The incoming light with wavelengths below 550 nm was completely absorbed by the photoanode material. As the sub-cells of the multijunction devices are electrically connected in series, the overall photocurrent of the photocathode will be defined by the smallest individual sub-cell *QE*. The limiting sub-cell for each cell type is highlighted by a green filling in Figure 3. A magnified view of each of the limiting *QE*s is shown in Figure S4, including the respective calculated photocurrent densities. The highest limiting sub-cell *QE* was provided by the a-Si:H/µc-Si:H/µc-Si:H solar cell with the hematite filter (bottom figure in Figure 3). In this configuration, the first a-Si:H absorber layer, whose light absorption was most affected by the hematite filter in all the tested cells, had a thickness of 160 nm and thus, was thicker than the a-Si:H top cells in the a-Si:H/a-Si:H and a-Si:H/a-Si:H/µc-Si:H configuration, respectively, with a thickness of 90 nm for both solar cells. This implied a better absorption of the incoming light and consequently a higher sub-cell *QE*. Increasing the thickness of the a-Si:H top cell layer beyond 160 nm would cause a spectral mismatching of the individual sub-cell photocurrent densities and thus, impair its performance. Nevertheless, beyond the aim of this study to present a proof of concept of a high current PEC-WS device, upcoming studies should focus on the optimization of the layer stack sequence and thicknesses, respectively, especially adapted for the combination with hematite-based light-absorbers. Moreover, other metal-oxide photoanodes could be combined with a multijunction thin-film silicon photocathode for PEC-WS. One salient candidate is $BiVO_4$ (bandgap energy ca. 2.3 - 2.4 eV), which, however, still suffers from poor electrochemical stability.[7,8]

3.3. Photoelectrochemical performance under light concentration

The photoelectrochemical performance of the filtered multijunction silicon photocathodes from Figure 4 and the hematite photoanode, respectively, is presented in Figure 4 (black curves). A nickel (Ni) foil on the surface of the silicon photocathodes served as HER catalyst (see experimental details in the SI). As expected from the *QE* measurements, the filtered a-Si:H/µc-Si:H/µc-Si:H photocathode (bottom figure in Figure 4) exhibited the highest photocurrent density among the tested silicon photocathodes of 1.8 mA/cm^2 at 0.8 V vs. RHE. Despite a lower onset-potential compared to the a-Si:H/a-Si:H/µc-Si:H photocathode and despite the lowest fill factor among the tested photocathodes (black solid curves), the crossing point of the a-Si:H/µc-Si:H/µc-Si:H photocathode with the hematite photoanode current-voltage (*j*-*V*) curve (dashed black curve) lied at the highest photocurrent density of 1.1 mA/cm^2, from

which an estimated solar-to-hydrogen (STH) efficiency of 1.35 % can be calculated. The photocurrent density at the crossing point for the a-Si:H/a-Si:H and the a-Si:H/a-Si:H/µc-Si:H photocathode was 0.7 mA/cm^2 and 0.9 mA/cm^2, respectively. Besides the fact that all the tested silicon photocathodes provided enough photovoltage to potentially enable bias-free water splitting using the hematite photoanode, the results of Figure 3 and Figure 4, respectively, furthermore demonstrate the high flexibility of multijunction thin-film silicon solar cells, regarding the adjustment of the photovoltage and photocurrent in a dual-absorber device.

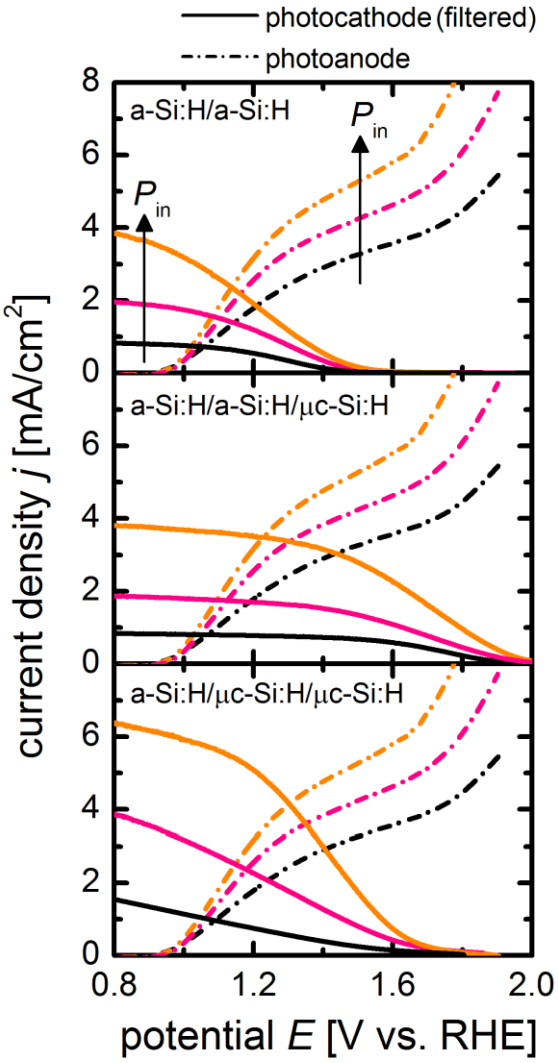

Figure 4. Linear sweep measurements of the three investigated thin-film silicon multijunction photocathodes (with hematite filter, solid lines): a-Si:H/a-Si:H, a-Si:H/a-Si:H/µc-Si:H, and a-Si:H/µc-Si:H/µc-Si:H, and the hematite photoanode (dashed lines) as a function of the illumination intensity (P_{in}). The measurements were conducted at 100 (black lines), 200 (purple lines), and 300 mW/cm^2 (orange lines) in 1 M NaOH electrolyte solutions using an Ag/AgCl reference electrode (3 M KCl). A Ni foil was used as HER catalyst for the tested photocathodes.

Nevertheless, in order to reach target hydrogen production required in industry or domestic usage, it is crucial to find ways to increase the bias-free photocurrent without expensive upscaling. The most efficient and straightforward method to do so, is to increase the available illumination intensity for the hybrid tandem device by light concentration.[14,15] In Figure 4, the effect of concentrated light illumination on the silicon photocathodes (solid curves) and on the photoanode (dashed curves) is shown.

We tested concentration factors of 2 and 3, giving illumination intensities P_{in} of 200 (purple curves) and 300 mW/cm^2 (orange curves), respectively. Please note that the light concentration was performed by approaching the hybrid tandem to the sun simulator and thus, might introduce some small deviations from the exact concentration factors, respectively. The strongest increase with light concentration in the photocurrent density at the crossing point of the photocathode and the photoanode *j-V* characteristics was obtained with the hematite/a-Si:H/µc-Si:H/µc-Si:H configuration. At 300 mW/cm^2 illumination intensity an estimated bias-free current density of 4.2 mA/cm^2 was deduced, corresponding to a STH efficiency of 1.72 % (calculated). Hence, a 27 % enhancement in the STH conversion efficiency can be deduced by increasing the illumination intensity from 100 to 300 mW/cm^2, stemming from an enhanced performance of both the photoanode and the filtered photocathode with increased P_{in}. As apparent from the *j-V* curves in Figure 4, the onset-potential of the photoelectrodes was not significantly affected by increased P_{in}. In fact, the value of the onset-potential depends much more on the internal structure of the solar cell, i.e. on the phenomena of recombination and charge transfer resistance.[16] Additionally, the photoelectrodes were heated up during concentrated illumination, which usually results in a slight decrease of the photovoltage.[15] Recombination and temperature effects therefore might have hampered a more pronounced increase in the onset-potential, as one would expect from semiconductor devices upon increased illumination intensity, i.e. in the presence of more photogenerated charge carriers.

The estimated bias-free photocurrent densities, as well as the deduced estimated STH efficiencies for all the investigated configurations as a function of the incident light intensity can be found in Figure 5. For the hematite/a-Si:H/µc-Si:H/µc-Si:H configuration, an increase in P_{in} not only augmented the photocurrent density, but also the fill factor of the filtered a-Si:H/µc-Si:H/µc-Si:H photocathode was significantly increased (bottom figure of Figure 4). This effect might be related to the fact that the recombination junctions at the different thin-film silicon sub-cell interfaces are very sensitive to light concentration, in particular at µc-Si:H/µc-Si:H junctions.[17] With the hematite photoanode as filter, this junction received a significantly reduced amount of light, which is why a lower amount of charge carriers was photogenerated, causing a higher resistance of the junction at 100 mW/cm^2 illumination intensity. By increasing the light concentration, losses related to the junction resistance were reduced, which resulted in a better fill factor for 300 mW/cm^2. This effect was also observable in the photovoltaic configuration (without electrolyte) as shown in Figure S5. Moreover, the increased light illumination could also heat up the surrounding electrolyte, which is conducive to improved electrochemical reaction kinetics, significantly reducing recombination losses due to improved charge transfer kinetics at the photoelectrode/electrolyte interface.[18]

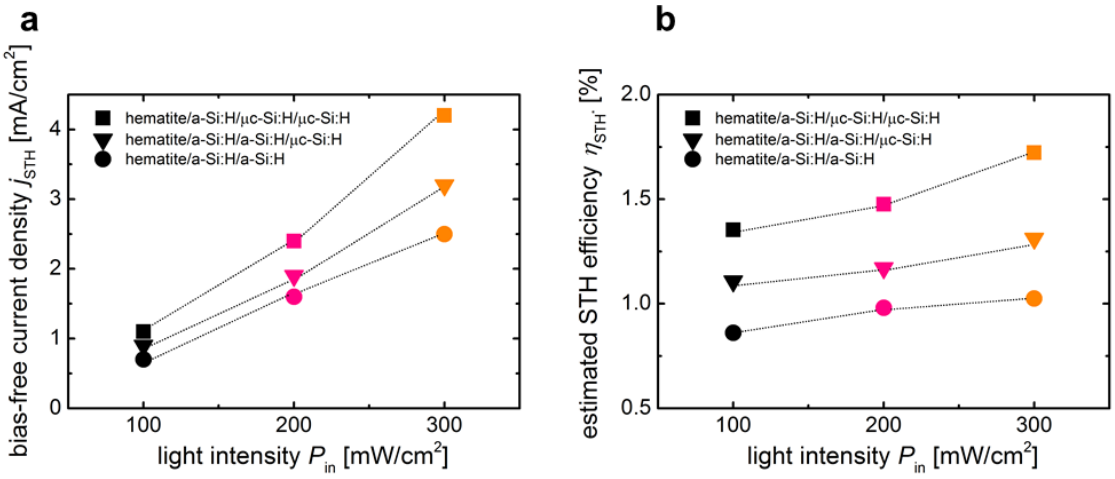

Figure 5. a) Photocurrent densities at the crossing points (i.e. estimated bias-free current densities) of the *j-V* characteristics of the filtered multijunction thin-film silicon photocathodes and the hematite photoanode, respectively, as a function of the incident light intensity P_{in}, obtained from Figure 4. b) Estimated solar-to-hydrogen (STH) efficiencies calculated from the values in a) as a function of the incident light intensity P_{in}.

3.4. HER catalysis optimization

The subsequent step consisted in further optimizing the hybrid tandem device regarding catalysis, especially for the HER. First of all, we tested higher electrolyte concentrations of the NaOH solution. The effect of NaOH concentrations of up to 6 M on the *j-V* characteristics of the filtered a-Si:H/μc-Si:H/μc-Si:H photocathode and the hematite photoanode, respectively, at 300 mW/cm^2 illumination intensity can be found in Figure S6a. The findings suggest that the photocurrent density at the crossing point of the photocathode and photoanode *j-V* curves, i.e. the estimated bias-free photocurrent remained unchanged with increasing NaOH concentration (Figure S6b). Therefore, we chose 1 M NaOH solution as the best choice to warrant an efficient and stable operation of the hybrid tandem device, avoiding issues, such as pitting corrosion or delamination of the active layers. Secondly, the aim was to enhance the HER catalysis by attaching a Ni foam (1.4 mm thick) on the flat Ni foil at the photocathode surface (by Ni epoxy). The three-dimensional (3-D) structure of the applied Ni foam offered a higher active surface area compared to the flat foil, which should be conducive to a better HER catalysis of the photocathode. This has been shown elsewhere[19-21] and was confirmed herein by the current density-potential *j*(*E*) measurement presented in Figure S7 in the SI, proving a shift of the onset potential for the cathodic current density in anodic direction as well as the steeper slope in the *j(E)* characteristics for the Ni foam compared to a Ni foil electrode. These results were reflected in the linear sweep curves shown in Figure 6, as the fill factor of the photocathode (filtered) significantly increased, indicating enhanced kinetics of the HER. As a consequence, the photocurrent density at the crossing point of the HER and OER curves was increased up to 4.6 mA/cm^2.

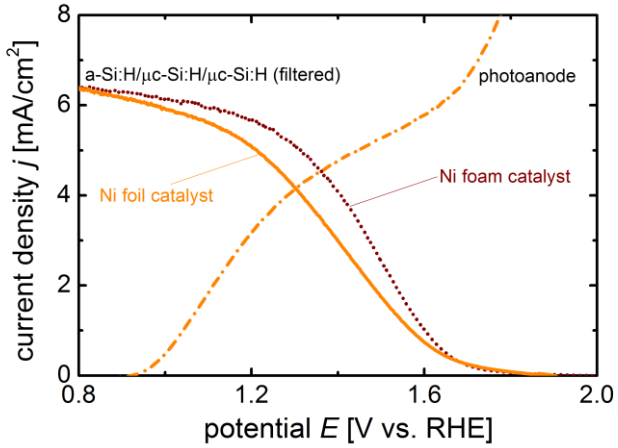

Figure 6. Linear sweep measurement of the a-Si:H/µc-Si:H/µc-Si:H (with hematite filter) photocathode and the hematite photoanode (orange dotted curve) under 300 mW/cm^2 illumination intensity. The linear sweep measurement of the photocathode was performed with a flat Ni foil catalyst (orange solid curve) and a 3-D Ni foam catalyst (dark red dotted curve). All measurements were conducted in 1 M NaOH electrolyte solutions using an Ag/AgCl reference electrode (3 M KCl).

3.5. Operation stability of hybrid tandem device

To confirm the results from Figure 6, obtained in the three-electrode configurations, we electrically connected the hematite photoanode to the a-Si:H/µc-Si:H/µc-Si:H/Ni photocathode, as shown in Figure 1, and measured the bias-free photocurrent density of the hybrid tandem device in two-electrode configuration under 300 mW/cm^2 illumination intensity. As apparent from Figure 7, the hematite/thin-film silicon PEC device exhibited unassisted solar water splitting with stable operation over more than 24 hours. In the first period of operation a bias-free photocurrent density of 4.6 mA/cm^2 was measured, as estimated from the three-electrode measurements in Figure 6.

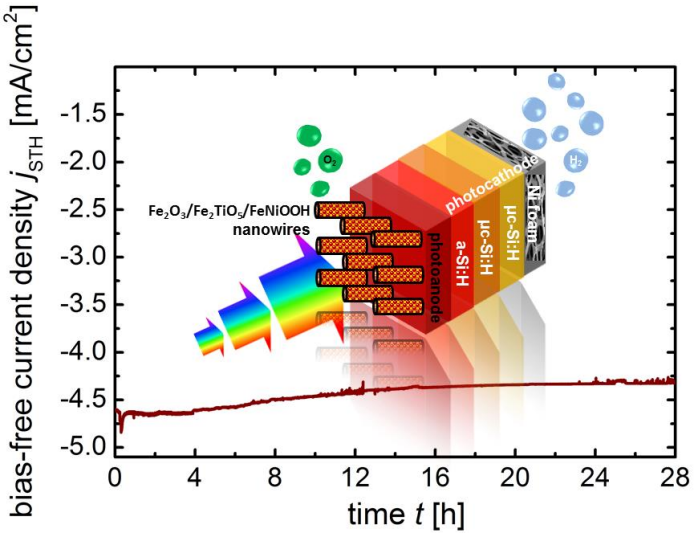

Figure 7. Net bias-free photocurrent density of the hybrid hematite/thin-film silicon tandem device under 300 mW/cm^2 illumination intensity in 1 M NaOH electrolyte solution. The measurement was conducted over more than 24 hours of operation. The inset schematically depicts the hybrid tandem configuration under operation.

After 28 hours of continuous PEC-WS operation, the hybrid tandem device showed a good robustness and 94 % of the initial bias-free photocurrent density was retained (4.3 mA/cm^2). Referring to the state-of-the-art oxide-based PEC-WS devices in literature, this is an outstanding bias-free photocurrent density, outperforming similar tandem device approaches, which usually operate at current densities below 1 mA/cm^2 (for 1-sun illumination intensity) and employ nobel metal catalysts.[7-9,22-29] Table S2 in the SI summarizes recent studies on hybrid tandem devices for unassisted water splitting. The long-term stability test confirmed that the Ni foil/Ni foam catalyst structure, as well as the hematite nanowire structures ensured an excellent protection of the photocathode and photoanode in harsh basic solutions (1 M NaOH), respectively. Figure 8a-d evidence that the nanowire multilayer composition, i.e. hematite core with the pseudobrookite protective coating was intact after the 28 hours stability test. Based on the HRTEM image of a nanowire edge in Figure 8a and the corresponding FFT spectrum in Figure 8b, the two indicated material phases could be deduced. Figure 8c depicts the corresponding IFFT RGB composition map of the HRTEM image (Figure 8a), showing the Fe_2O_3 core and the Fe_2TiO_5 surrounding layer. The FeNiOOH nanoparticles also showed an excellent robustness, as they could be detected on the pseudobrookite surface after the stability test, as shown by the EELS signals in Figure 8d (lower right map) and in the TEM and HRTEM analysis in Figure S8, respectively. Furthermore, the EELS maps of the photoanode nano-structure before and after the stability test were in perfect agreement (Figure S2 vs. Figure 8d), which confirmed the high robustness of the photoanode nano-structures.

Consequently, the slight observable decrease in the bias-free photocurrent density in Figure 7 (less than 6 % over 28 hours operation) presumably originated from degradations of the photocathode. One critical point to consider is the heating up of the photocathode. In continuous operation with concentrated illumination, the temperature of the photocathode will inevitably increase, which in general results in a slight decrease of the photovoltage, due to changes in the bandgap energies of the thin-film silicon absorber layers.[15,30] This effect might have shifted the operation point of the hybrid PEC-WS device into lower current density region. Another possible explanation would be that light-induced degradation (LID) of the thin-film silicon material could have affected the long-term performance of the photocathode.[31] It is well accepted that LID could decrease the performance of thin-film silicon devices. Studies evidence, that in particular the fill factor of the devices is negatively affected, which would be to the detriment of the operation point of the hybrid tandem device. Nevertheless, it was shown that the effect of LID is less pronounced for µc-Si:H than for a-Si:H layers, which is why a-Si:H/µc-Si:H/µc-Si:H structures are less affected by LID than a-Si:H/a-Si:H/µc-Si:H or a-Si:H/a-Si:H multijunctions, having two a-Si:H absorber layers.[31]

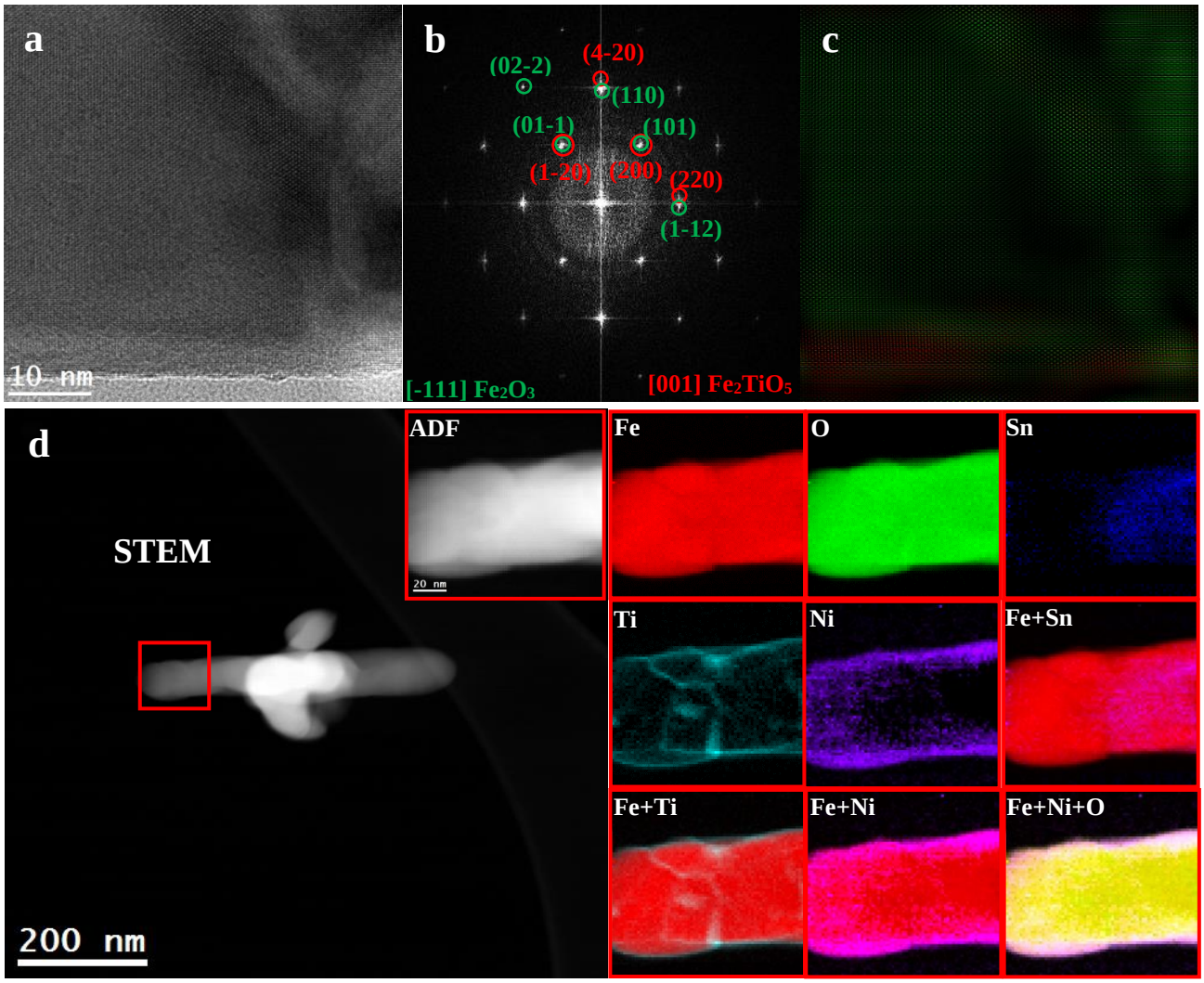

Figure 8. a) High resolution TEM image of a hematite nanowire after the 28 hours operation stability test (Figure 7) area showing the hierarchal structure of the nanowire composite. b) Corresponding FFT spectrum of a) indicating that the nanowire is composited of hematite and pseudobrookite visualized along [-111] and [001] directions, respectively. c) Phase map obtained from a) after mask filtering the corresponding spots for each of the phases in b) and obtaining their corresponding IFFT RGB composite image. d) EELS chemical composition maps obtained from the red rectangled area of the annular dark-field (ADF)-STEM micrograph (left), showing a multilayer nanowire (after the stability test). Individual Fe (red), O (green), Sn (blue), Ti (indigo), and Ni (purple) maps and their composite.

4. Discussion

The laboratory-scale device presented in this study was designed from components which can be scaled up to larger PEC-WS systems. Furthermore, we note that only earth-abundant materials (absorbers and catalysts) were applied, which potentially enable the deployment of economical large-scale installations. Nevertheless, foregoing the usage of nobel metal catalysts (e.g. Pt or RuO_2) and expensive photovoltaic structures (e.g. multijunction III-V) inevitably implies limitations in the electrochemical reaction kinetics and achievable photocurrents, respectively. To circumvent this tradeoff for PEC-WS between economic viability and high yield H_2 production, the herein

proposed concept of light concentration might be of significant interest. In particular tandem systems can profit from light concentration approaches, because in this case both absorber layers can profit from increased light intensity boosting the operative photocurrent density even more compared to decoupled photoanode-cathode of anode-photocathode systems, respectively, were the performance of only one component will be enhanced.

Nevertheless, it should be noted that the presented analysis (as well as the majority of the related studies) assumes that the concentrated light on the hybrid tandem device cell is the only energy input into the system. In reality, however, there can be additional energy inputs, including the energy required to continuously flow the electrolyte (e.g. for gas bubble removal) and heat management. For large-scale concentrated PEC-WS devices there may also be optical losses in the lenses or mirrors used to concentrate the incident sunlight onto the light absorber, which could reduce the system efficiency. In fact, we chose to neglect these aspects in our investigation, mainly because of two reasons: i) For the sake of comparison with results from previous studies and ii) because the losses in a laboratory-scale demonstration system are less relevant, in addition to being more difficult to accurately quantify. As a result, the herein reported bias-free photocurrent represents a limiting upper bound with respect to any additional auxiliary energy inputs that would be required for any commercially scaled concentrated PEC-WS system.
Moreover, the backward reaction, i.e. the recombination of hydrogen and oxygen into water can impair the overall STH efficiency. The next immediate step would therefore be to implement a gas separation membrane for the upscaled design, such as reported by Verlage *et al.*[32] In this regard, also the addition of carbonate salts or other electron mediators in the electrolyte could prevent backward reaction and thereby enhance the hydrogen production rate.[33,34]
Overall, the goal of every solar-driven H_2 generation system is to minimize the levelized cost of hydrogen produced over the operating lifetime of the system. Although the photocurrent densities achieved with the presented hybrid tandem device are low compared to decoupled EC-PV systems,[35] the low-cost and scalable approach that this strategy offers may have the potential to produce hydrogen at an equivalent cost. Furthermore, when thinking of a sort of "PEC farm" constituted of many upscaled PEC-WS devices for H_2 production, the lower photocurrent densities could be beneficial regarding lower overpotential losses and thus, eventually higher efficiencies. In this regard, it is projected by techno-economic models of large scale, centralized solar H_2 production facilities that overpotential losses at high operating current densities are one of the most important factors in reducing the STH efficiency and thus, increasing the cost of H_2.[36,37] Therefore, continued development of more efficient optical coupling of hybrid tandem partners by tuning of the functional layers and sub-cell currents and technoeconomic models to predict hydrogen costs are all important subjects for continuing research in PEC-WS.

5. Conclusion

In summary, we presented an efficient and scalable approach for PEC-WS, which only makes use of low-cost and earth-abundant absorber and non-nobel catalyst materials. The concept of light concentration was successfully introduced for hybrid devices for solar hydrogen production, which effectively could increase the bias-free

photocurrent density and thus, the STH efficiency of the dual-absorber tandem device, which was increased by 27 %. In the optimized PEC-WS device configuration, a bias-free photocurrent density of 4.6 mA/cm^2 was achieved over a prolonged period of operation (28 hours). In conclusion, this study can serve as proof of concept that the promises of oxide-based devices for solar water splitting, regarding price, photocurrents, and stability can be fulfilled while keeping PEC-WS on course towards a viable alternative to other pathways of solar hydrogen production.

Acknowledgment

Authors acknowledge funding from Generalitat de Catalunya through the CERCA program, 2017 SGR 1246, 2017 SGR 327 and the Spanish MINECO projects MAT2014-59961, ENE2016-80788-C5-5-R and ENE2017-85087, together with the support from REPSOL, S. A. ICN2 is supported by the Severo Ochoa program from Spanish MINECO (Grant No. SEV-2017-0706). IREC also acknowledges additional support from the European Regional Development Funds (ERDF, FEDER), (S)TEM part of the present work has been performed in the framework of Universitat Autònoma de Barcelona Materials Science PhD program and the rest in the Nanoscience program of the University of Barcelona. The authors thank S. Moll (IEK-5), M. Biset-Peiró (IREC), and H. Xie (IREC) for their contribution to this work. F.U. acknowledges financial support from MINECO through Juan de la Cierva fellowship (FJCI-2016-29147).V.S., K.W., and F.F. (authors from IEK-5) thank the Deutsche Forschungsgemeinschaft (DFG) (Priority Program SPP 1613).

Author contributions

F.U. and J. R. M. conceived the project and designed the experiments. F.U. carried out the (photo)-electrochemical experiments. P.Y.T. and J.A. conducted the structural and compositional analyses and prepared the photoanode material. F.U. and P.Y.T. interpreted data. F.U. wrote the manuscript. V.S., K.W., and F.F. performed the deposition and characterization (*QE* and *j-V*) of the multijunction thin-film silicon solar cells. J.R.M. and T.A. supervised the proposed and executed research program. All the authors participated in discussions and contributed to editing of the manuscript.

References

[1] T. J. Jacobsson, *Energy Environ. Sci*. **2018**, *11*, 1977.

[2] M. R. Shaner, H. A. Atwater, N. S. Lewis, E. W. McFarland, *Energy Environ. Sci.* **2016**, *9*, 2354.

[3] S. Dahl, I. Chorkendorff, *Nat. Mater*. **2012**, *11*, 100.

[4] A. C. Nielander, M. R. Shaner, K. M. Papadantonakis, S. A. Francis, N. S. Lewis, *Energy Environ. Sci*. **2015**, *8*, 16.

[5] K. Sivula, F. Le Formal, M. Grätzel, *ChemSusChem* **2011**, *4*, 432.

[6] P. Tang, H. Xie, C. Ros, L. Han, M. Biset-Peiró, Y. He, W. Kramer, A. Pérez Rodríguez, E. Saucedo, J.R. Galán-Mascarós, T. Andreu, J. R. Morante, J. Arbiol, *Energy Environ. Sci*. **2017**, *10*, 2124.

[7] F. Urbain, V. Smirnov, J.-P. Becker, A. Lambertz, F. Yang, J. Ziegler, B. Kaiser, W. Jaegermann, U. Rau, F. Finger, *Energy Environ. Sci*. **2016**, *9*, 145.

[8] J.-W. Jang, C. Du, Y. Ye, Y. Lin, X. Yao, J.Thorne, E. Liu, G. McMahon, J. Zhu, A. Javey, J. Guo, D. Wang, *Nat. Comm*. **2015**, *6*, 7447.

[9] P. Xu, J. Feng, T. Fang, X. Zhao, Z. Li, Z. Zouab, *RSC Adv*. **2016**, *6*, 9905.

[10] N. Kornienko, N. A. Gibson, H. Zhang, S. W. Eaton, Y. Yu, S. Aloni, S. R. Leone, P. Yang, *ACS Nano* **2016**, *10*, 5525.

[11] F. Urbain F, K. Wilken, V. Smirnov, O. Astakhov, A. Lambertz, J.-P. Becker, U. Rau, J. Ziegler, B. Kaiser, W. Jaegermann, F. Finger, *Int. J. Photoenergy* **2014**, *2014*, 249317.

[12] F. Urbain, V. Smirnov, J.-P. Becker, U. Rau, F. Finger, J. Ziegler, B. Kaiser, W. Jaegermann, *J. Mater. Res*. **2014**, *29*, 2605.

[13] B. Iandolo, B. Wickman, I. Zorić, A. Hellman, *J. Mater. Chem. A* **2015**, *3*, 16896.

[14] A. Royne, C. J. Dey, D. R. Mills, *Sol. Energy Mater. Sol. Cells* **2005**, *86*, 451.

[15] F. Urbain, S. Murcia-López, N. Nembhard, J. Vázquez-Galván, C. Flox, V. Smirnov, K. Welter, T. Andreu, F. Finger, J. R. Morante, *J. Phys. D: Appl. Physics* **2018**, *52*, 4.

[16] D. Klotz, D. Shai Ellis, H. Dotan, A. Rothschild, *Phys. Chem. Chem. Phys.* **2016**,*18*, 23438.

[17] I. A. Yunaz, A. Yamada, M. Konagai, *Jpn. J. Appl. Phys*. **2007**, *46*, 45.

[18] Y. Pihosh, I. Turkevych, K. Mawatari, J. Uemura, Y. Kazoe, S. Kosar, K. Makita, T. Sugaya, T. Matsui, D. Fujita, M. Tosa, M. Kondo, T. Kitamori, *Sci. Reports* **2015**, *5*, 11141.

[19] J. Lu, T. Xiong, W. Zhou, L. Yang, Z. Tang, S.Chen, *ACS Appl. Mater. Interfaces* **2016**, *8*, 5065.

[20] B. Turan, J.-P. Becker, F. Urbain, F. Finger, U. Rau, S. Haas S, *Nat. Comm*. **2016**, *7*, 12681.

[21] F. Urbain, P. Tang, N. M. Carretero, T. Andreu, L. G. Gerling, C. Voz, J. Arbiol, J. R. Morante, *Energy Environ. Sci*. **2017**, *10*, 2256.

[22] P. Bornoz, F. F. Abdi, S. D. Tilley, B. Dam, R. van de Krol, M. Graetzel, K. Sivula, *J. Phys. Chem. C* **2014**, *118*, 16959.

[23] F. Jiang, Gunawan, T. Harada, Y. Kuang, T. Minegishi, K. Domen, S. Ikeda, *J. Am. Chem. Soc.* **2015**, *137*, 13691.

[24] H. Kaneko, T. Minegishi, M. Nakabayashi, N. Shibata, Y. Kuang, T. Yamada, K. Domen, *Adv. Funct. Mater*. **2016**, *26*, 4570.

[25] J. H. Kim, H. Kaneko, T. Minegishi, J. Kubota, K. Domen, J. S. Lee, *ChemSusChem* **2016**, *9*, 61.

[26] T. Higashi, H. Kaneko, T. Minegishi, H. Kobayashi, M. Zhong, Y. Kuang, T. Hisatomi, M. Katayama, T. Takata, H. Nishiyama, T. Yamada, K. Domen, *Chem. Commun*. **2017**, *53*, 11674.

[27] Y. Goto, T. Minegishi, Y. Kageshima, T. Higashi,H. Kaneko,Y. Kuang, M. Nakabayashi, N. Shibata, H. Ishihara, T. Hayashi, A. Kudo, T. Yamadaa, K. Domen, *J. Mater. Chem. A* **2017**, *5*, 21242.

[28] A. Iwase, A. Kudo, Y. Numata, M. Ikegami, T. Miyasaka, N. Ichikawa, M. Kato, H. Hashimoto, H. Inoue, O. Ishitani, H. Tamiaki, *ChemSusChem* **2017**, *10*, 4420.

[29] L. Pan, J. H. Kim, M. T. Mayer, M.-K. Son, A. Ummadisingu, J. S. Lee, A. Hagfeldt, J. Luo, M. Grätzel, *Nat. Catal*. **2018**,*1*, 412.

[30] F. Urbain, J.-P. Becker, V. Smirnov, J. Ziegler, F. Yang, B. Kaiser, W. Jaegermann, S. Hoch, A. Maljusch, U. Rau, F. Finger, *Mater. Sci. Sem. Proces* **2017**, *42*, 142.

[31] F. Urbain, V. Smirnov, J.-P. Becker, F. Finger, *ACS Omega* **2016**, *1*, 832.
[32] E. Verlage, S. Hu, R. Liu, R. J. R. Jones, K. Sun, C. Xiang, N. S. Lewis, H. A. Atwater, Energy Environ. Sci. **2015**, *8*, 3166.
[33] M. Ni, M. K. H. Leung, D. Y. C. Leung, K. Sumathy, Renew. Sustain. Energy Rev. **2007**, *11*, 401.
[34] R. Abe, K. Sayama, H. Arakawa, Chem. Phys. Lett. **2003**, *371*, 360.

[35] J. Jia, L. C. Seitz, J. D. Benck, Y. Huo, Y. Chen, J. Wei Desmond Ng, T. Bilir, J. S. Harris, T. F. Jaramillo, *Nat. Comm*. **2016**, *7*, 13237.

[36] B. M. Klahr, D. Peterson, K. Randolph, E. L. Miller, *ECS Trans*. **2017**, *75*, 3.

[37] J. H. Montoya, L. C. Seitz, P. Chakthranont, A. Vojvodic, T. F. Jaramillo, J. K. Nørskov, *Nat. Mat*. **2017**, *16*, 70.